



CHALMERS

Chalmers Publication Library

Quantum Hall effect in graphene decorated with disordered multilayer patches

This document has been downloaded from Chalmers Publication Library (CPL). It is the author's version of a work that was accepted for publication in:

Applied Physics Letters (ISSN: 0003-6951)

Citation for the published paper:

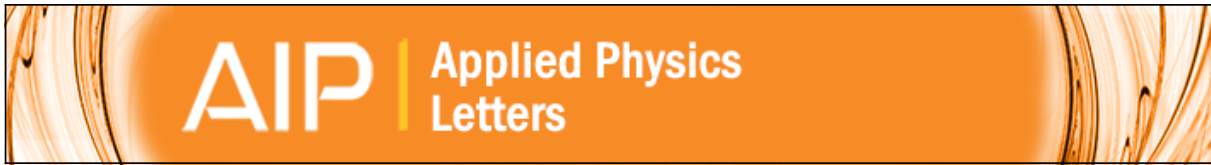
Nam, Y. ; Sun, J. ; Lindvall, N. (2013) "Quantum Hall effect in graphene decorated with disordered multilayer patches". Applied Physics Letters, vol. 103(233), pp. 233110.

Downloaded from: <http://publications.lib.chalmers.se/publication/190547>

Notice: Changes introduced as a result of publishing processes such as copy-editing and formatting may not be reflected in this document. For a definitive version of this work, please refer to the published source. Please note that access to the published version might require a subscription.

Chalmers Publication Library (CPL) offers the possibility of retrieving research publications produced at Chalmers University of Technology. It covers all types of publications: articles, dissertations, licentiate theses, masters theses, conference papers, reports etc. Since 2006 it is the official tool for Chalmers official publication statistics. To ensure that Chalmers research results are disseminated as widely as possible, an Open Access Policy has been adopted. The CPL service is administrated and maintained by Chalmers Library.

(article starts on next page)



Quantum Hall effect in graphene decorated with disordered multilayer patches

Youngwoo Nam, Jie Sun, Niclas Lindvall, Seung Jae Yang, Dmitry Kireev, Chong Rae Park, Yung Woo Park, and August Yurgens

Citation: [Applied Physics Letters](#) **103**, 233110 (2013); doi: 10.1063/1.4839295

View online: <http://dx.doi.org/10.1063/1.4839295>

View Table of Contents: <http://scitation.aip.org/content/aip/journal/apl/103/23?ver=pdfcov>

Published by the [AIP Publishing](#)



Re-register for Table of Content Alerts

Create a profile.



Sign up today!



Quantum Hall effect in graphene decorated with disordered multilayer patches

Youngwoo Nam,^{1,2,a)} Jie Sun,^{2,b)} Niclas Lindvall,² Seung Jae Yang,³ Dmitry Kireev,² Chong Rae Park,³ Yung Woo Park,¹ and August Yurgens²

¹Department of Physics and Astronomy, Seoul National University, Seoul 151-747, South Korea

²Department of Microtechnology and Nanoscience, Chalmers University of Technology, SE-412 96 Gothenburg, Sweden

³Department of Materials Science and Engineering, Seoul National University, Seoul 151-747, South Korea

(Received 6 October 2013; accepted 17 November 2013; published online 5 December 2013)

Quantum Hall effect (QHE) is observed in graphene grown by chemical vapour deposition using platinum catalyst. The QHE is even seen in samples which are irregularly decorated with disordered multilayer graphene patches and have very low mobility ($<500 \text{ cm}^2\text{V}^{-1}\text{s}^{-1}$). The effect does not seem to depend on electronic mobility and uniformity of the resulting material, which indicates the robustness of QHE in graphene. © 2013 AIP Publishing LLC.

[<http://dx.doi.org/10.1063/1.4839295>]

The integer quantum Hall effect (QHE) is a hallmark of a two-dimensional (2D) electron gas formed at the interface between semiconductors or their surfaces.¹ Graphene is a perfect 2D material.² Unlike the conventional 2D electron gas, graphene shows a half-integer QHE due to a Berry's phase π .³ The half-integer QHE in graphene demonstrates not only the 2D nature of graphene but also its unique Dirac-like electronic structure associated with the spin- and valley-degeneracy and the feature of the central Landau level (LL) where electrons and holes coexist.

Generally, in order to observe the QHE, three essential conditions are required: low temperatures ($<4 \text{ K}$), high magnetic fields ($\geq 10 \text{ T}$), and clean samples with high mobility ($>10^3 \text{ cm}^2\text{V}^{-1}\text{s}^{-1}$). This makes LLs more discrete by decreasing the width of LLs and increasing the energy spacing between adjacent LLs. Indeed, most of QHE experiments (including fractional QHE) on graphene were performed under these conditions.³⁻⁷ Exceptionally, graphene QHE was observed even at room-temperature⁸ explained by the fact that graphene innately has an unequal energy spacing between LLs and an anomalously large energy spacing between the central LL and its nearest LLs, compared to an ordinary 2D electron gas. The ultra-high magnetic field ($\sim 30 \text{ T}$) and notably high mobility of the sample ($>10^4 \text{ cm}^2\text{V}^{-1}\text{s}^{-1}$) used in this experiment also enable the QHE to appear at room temperature. Meanwhile, the weak QHE associated with relatively low mobility 2D gas system is usually employed to study a magnetic field induced transition from the Anderson localization (insulator) to quantum Hall state (conductor).⁹ Recently, the transition was also observed in low mobility graphene ($\sim 900 \text{ cm}^2\text{V}^{-1}\text{s}^{-1}$) grown on silicon carbide.¹⁰

The width Γ of LLs and the energy spacing ΔE between LLs are determined by the mobility μ and magnetic field B . The high mobility assures the small Γ because of the uncertainty relation $\Gamma \cdot \tau \sim \hbar$, where \hbar is the reduced Planck's

constant and τ is the momentum relaxation time, which is proportional to the mobility. The high magnetic field increases ΔE ($=\hbar\omega_c$) since the cyclotron frequency ω_c is proportional to the magnetic field. Hence, ΔE needs to be much larger than Γ for observing the QHE, which results in the condition, $\omega_c\tau = \mu B \gg 1$ corresponding to $\mu > 1000 \text{ cm}^2\text{V}^{-1}\text{s}^{-1}$ at $B = 10 \text{ T}$.

Accordingly, most of the previous QHE experiments on graphene were performed using mechanically exfoliated graphene with high mobility exceeding $10^4 \text{ cm}^2\text{V}^{-1}\text{s}^{-1}$.³⁻⁷ However, there have been some reports on QHE in graphene grown by chemical vapour deposition (CVD) using nickel-¹¹ and copper-catalyst.¹² Although the QHE in the CVD-graphene was not as clear as in exfoliated one, the relatively high mobility of such a graphene ($>3000 \text{ cm}^2\text{V}^{-1}\text{s}^{-1}$) ensures seeing QHE. Recently, CVD-graphene on Pt was also grown and investigated,¹³⁻¹⁵ although no QHE in such a graphene has so far been reported in the literature. Graphene grown on Pt can have millimetre-sized hexagonal single-crystal grains and mobility greater than $7000 \text{ cm}^2\text{V}^{-1}\text{s}^{-1}$ (Ref. 14), promising clear QHE in such samples.

Here, we experimentally confirm the half-integer QHE in CVD-graphene grown on platinum in the magnetic field $B > 11 \text{ T}$. Surprisingly, we observe the QHE even in samples which are irregularly decorated with disordered multilayer graphene patches (see Fig. 1(a)) and have very low mobility ($<500 \text{ cm}^2\text{V}^{-1}\text{s}^{-1}$). This emphasizes the robustness of QHE in Pt-CVD graphene.

The graphene is synthesised in a cold-wall low-pressure CVD system¹⁶ equipped with a small-mass graphite heater. A $100 \mu\text{m}$ -thick polycrystalline Pt foil (99.99%) is employed as catalyst. First, we ramp up the temperature of the foil to 1000°C at $300^\circ\text{C}/\text{min}$ and hold it at this temperature for 5 min in a flow of 1000 sccm H_2 . Then, 70 sccm CH_4 pre-diluted with Ar to 5% is introduced into the chamber to activate graphene growth. The growth time is 10 min. Finally, the foil is cooled down to below 100°C within 15 min by turning off the heater current. The CH_4 is kept flowing while cooling down. We note that the growth temperature of 1000°C is the nominal temperature obtained from a

^{a)}Author to whom correspondence should be addressed. Electronic mail: youngwoo.nam@chalmers.se

^{b)}Electronic mail: jie.sun@chalmers.se

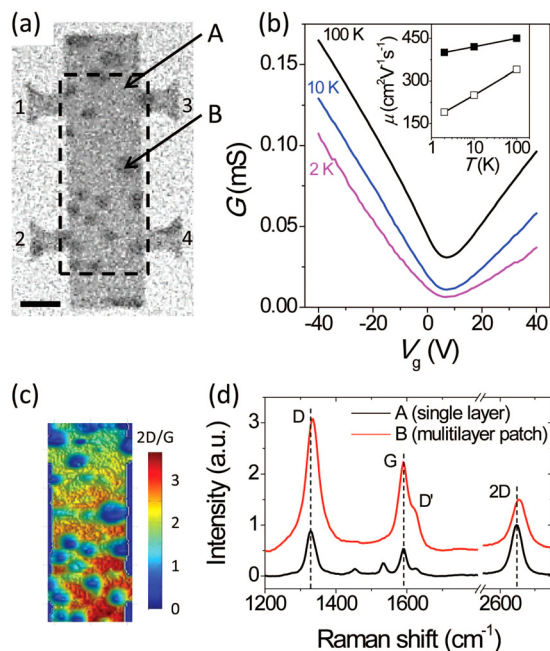


FIG. 1. (a) An optical image of the Hall-bar shaped graphene decorated with multilayer patches. The scale bar is $5\ \mu\text{m}$. (b) The conductance G versus gate voltage V_g at temperature $T=100, 10,$ and $2\ \text{K}$. The solid- and open-squares in the inset show the temperature-dependent mobility μ for electrons and holes, respectively. The mobility decreases with decreasing temperature. The hole- and electron-mobility at $T=2\ \text{K}$ are 400 and $190\ \text{cm}^2\text{V}^{-1}\text{s}^{-1}$, respectively. The Hall mobility is independent of the voltage-contact pairs (1 and 3 or 2 and 4 in Fig. 1(a)). (c) Mapping of Raman intensity ratio between 2D- and G-bands for graphene region enclosed by dashed line in (a). (d) The Raman spectra of graphene at two sites denoted by arrows in (a): A (single layer graphene) and B (multilayer graphene patch). Both spectra are normalized to 2D-band intensity and spectrum B is shifted upwards for clarity.

thermocouple sensor gently touching the heater. The actual catalyst temperature can be $100\text{--}200\ ^\circ\text{C}$ higher.¹⁷ The high melting point ($\sim 1770\ ^\circ\text{C}$) of Pt enables us to access high temperature over $1000\ ^\circ\text{C}$, which is impossible to achieve with conventional Cu catalyst. In addition to the high temperature $>1000\ ^\circ\text{C}$, we use a low partial pressure of the precursor gas, different from the previous graphene growth on Pt,^{14,15} performed under atmospheric pressure and temperature $\sim 1000\ ^\circ\text{C}$.

We notice that changing the flow rate of CH_4 to somewhat in excess of $\sim 50\ \text{sccm}$ gives rise to additional multilayer graphene patches of $\sim 5\ \mu\text{m}$ in size (Fig. 1(a)), whereas the overflow of CH_4 ($>100\ \text{sccm}$) generates much thicker and larger multilayer patches. This means that the thickness and size of the patches are controllable by the flow rate of CH_4 .

Afterwards, the graphene is transferred onto a highly doped Si substrate capped with $300\ \text{nm}\ \text{SiO}_2$, allowing for a field-effect transistor structure. We employ the frame-assisted bubbling transfer technique^{14,18} instead of usual wet etching of the metal catalyst thereby avoiding etching residues and possible damage of graphene caused by strong acids as in the case of Pt catalyst. The semi-rigid frame supporting the PMMA coated graphene allows for easy handling and cleaning of graphene.¹⁸ Using the frame, we can rinse graphene more thoroughly during the transfer process. Finally, graphene Hall bar structures ($\sim 10 \times 40\ \mu\text{m}^2$) are patterned using a standard micro fabrication process.

The resistance measurements are carried out using a current-reversing dc technique with a bias current of $100\ \text{nA}$. In addition, the measurements are done both at positive and negative magnetic fields to be able to eventually compensate for a small misalignment of the Hall contacts.

Fig. 1(a) shows an optical image of our graphene sample placed on the SiO_2/Si substrate. The image contrast is sufficient to discern the boundary of graphene and its inhomogeneous structure. We can see that relatively dark patches ($<5\ \mu\text{m}$) are scattered all over the sample. The patchy structure is made by increasing the flow rate of CH_4 to about $70\ \text{sccm}$ during the growth process compared to the optimal flow rate of $\text{CH}_4 \sim 50\ \text{sccm}$ for growing a single-layer graphene without patches. If we further increased the flow rate of CH_4 , much thicker pyramid-like patches would be formed, where several graphene layers would be clearly distinguishable.

We measure the 4-probe conductance of graphene at different charge carrier densities by tuning the gate voltage at the temperature $T=100, 10,$ and $2\ \text{K}$ (see Fig. 1(b)). The conductance curves show a p-type doping (Dirac point $V_{\text{DP}} \sim +6.5\ \text{V}$); their shape is independent of the voltage-contact pairs (1 and 2 or 3 and 4 in Fig. 1(a)). Thus, the patches do not appear to affect the overall average conductance of the sample. The conductance has a positive temperature dependence ($dG/dT > 0$) in the whole range of the gate voltage. This agrees with the previous results on defective graphene deliberately damaged by the hydrogenation¹⁹ or ion irradiation.²⁰ The positive temperature dependence in our case can also be associated with the inhomogeneity of our sample and explained by the heterogeneous model of variable-range hopping where well conducting regions (single layer graphene) are separated by less conducting regions (multilayer patches).²¹

The slope of conductance curves allows for rough estimates of the mobility at different temperatures (see the inset of Fig. 1(b)). In contrast to usually enhanced mobility of monolayer graphene at lower temperature, the mobility of this sample decreases with decreasing temperature, which results in the mobility $\mu \sim 400$ and $190\ \text{cm}^2\text{V}^{-1}\text{s}^{-1}$ at $T=2\ \text{K}$ for holes and electrons, respectively. The temperature dependence of mobility is analogous to that of multilayer graphene where Coulomb scattering is dominant and the substrate surface polar phonon induced electric field is screened by extra graphene layers.²² Hence, we believe that our positive temperature dependence of mobility can be associated with the multilayer patches in the sample. Here, we use a parallel-electrode capacitance model.² The Hall mobility for the holes is $\sim 310\ \text{cm}^2\text{V}^{-1}\text{s}^{-1}$, which is comparable with the field-effect result. It is a very low mobility compared to the previously reported graphene field effect devices in literatures. The low mobility cannot be only attributed to the presence of the defective patches because the distance between them is rather big. Even in the predominantly single-layer areas (region A), the graphene is quite disordered as seen in the Raman spectra in Fig. 1(d).

In an effort to identify the patch composition, Raman spectroscopy is performed. Fig. 1(c) indicates mapping of Raman intensity ratio between 2D- and G-bands for graphene region enclosed by dashed line in Fig. 1(a). We find that the intensity ratio of graphene patches (blue round

regions) is smaller than one. Fig. 1(d) shows Raman spectra from different sample parts denoted in Fig. 1(a): A (outside the patch) and B (at the patch). The spot A demonstrates a typical Raman spectrum characteristic for a disordered single layer graphene with exception for additional peaks between D and G bands. The peaks can be caused by amorphous (hydrogenated) carbon formed during sample growth or device fabrication.²³ The Raman spectrum in region B displays a much stronger intensity of both D-band (related to the inter-valley scattering process) and D'-band (associated with the intra-valley scattering process in graphene) compared to that of the single layer region A. This indicates that graphene is much more disordered in patch spot B than in single-layer area A. In addition, the spectrum obtained from the patch shows a broader 2D-band accompanied with blue shift ($\sim +7.1 \text{ cm}^{-1}$) and lower ratio of I_{2D} to I_G . This is consistent with the signature of multi-layer graphene.²⁴ Therefore, we conclude that the dark patches consist of a defective multi-layer graphene.

We now turn to QHE measurements. In general, it is known that single-layer graphene shows the half-integer QHE conductance plateaus $\sigma_{xy} = \pm 4(n + 1/2)e^2/h \equiv \nu e^2/h$ with the non-negative integer n and filling factors $\nu = \pm 2, \pm 6, \pm 10, \dots$. The integer step of 4 in ν is a manifestation of the four-fold degeneracy of graphene LL owing to the spin- and valley-degeneracy. Occasionally, high quality graphene shows other integer ν owing to symmetry breaking;^{4,5} even fractional ν can sometimes be found.^{6,7}

Figs. 2(a) and 2(b) show the longitudinal resistance R_{xx} and Hall resistance R_{xy} as a function of the gate voltage measured at the magnetic field $B = 14 \text{ T}$ and $T = 2 \text{ K}$. We can see that the longitudinal resistance R_{xx} abruptly drops to nearly zero (160 Ω and 530 Ω for holes and electrons) whereas R_{xy} reaches the quantum Hall plateaus at $\nu = \pm 2$ corresponding to $\approx \pm 12.9 \text{ k}\Omega$. The slight deviation of the measured values ($-12.5 \text{ k}\Omega$ and $+12.3 \text{ k}\Omega$ for holes and electrons) from the exact QHE plateau value is caused by the

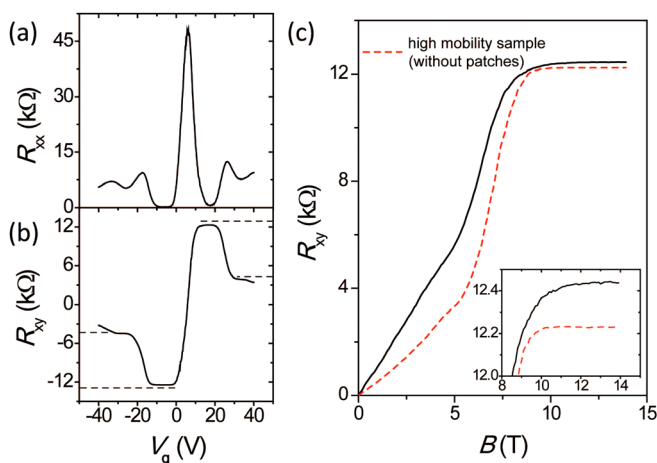


FIG. 2. (a) The longitudinal resistance R_{xx} and (b) Hall resistance R_{xy} as a function of gate voltage at magnetic field $B = 14 \text{ T}$ and $T = 2 \text{ K}$. Both R_{xx} and R_{xy} are independent of the voltage-contact pairs (1 and 2 or 3 and 4 for R_{xx} and 1 and 3 or 2 and 4 for R_{xy} , see Fig. 1(a)). Quantum Hall resistance of $\pm h/2e^2$ ($\approx \pm 12.9 \text{ k}\Omega$) and $\pm h/6e^2$ ($\approx 4.30 \text{ k}\Omega$) are denoted as horizontal dashed lines in (b). (c) R_{xy} versus B at $V_g = -6 \text{ V}$. The dashed red line corresponds to the high mobility sample which has no patches. The inset shows quantum Hall plateaus in the zoomed-in region.

external shunting resistors of $1 \text{ M}\Omega$ connecting all the electrodes together to avoid occasional sample damage due to discharges. The deviation can also be a result of incompleteness of the quantum Hall state in our system as indicated by the non-zero R_{xx} . The presence of bilayer regions can be the cause of such a situation.²⁵ Besides, a weak signature of the plateaus at $\nu = \pm 6$ ($\approx 4.30 \text{ k}\Omega$) can be found together with a slight dip in R_{xx} . The higher-order plateaus cannot be seen much likely due to disorder-induced broadening of the LLs at higher energy. The QHE is seen more clearly on the hole side due to the higher mobility of holes ($400 \text{ cm}^2\text{V}^{-1}\text{s}^{-1}$) compared to the mobility of electrons ($190 \text{ cm}^2\text{V}^{-1}\text{s}^{-1}$).

Evolution of the quantum Hall plateaus with magnetic field is shown in Fig. 2(c). For comparison, we prepare a uniform monolayer (non-patched) Pt-CVD graphene using reduced flow rate of $\text{CH}_4 \sim 50 \text{ sccm}$. The sample shows a relatively high mobility $\mu \sim 2000 \text{ cm}^2\text{V}^{-1}\text{s}^{-1}$; its QHE is denoted as dashed red line. The QHE measurements for both patched (low mobility)- and non-patched (high mobility)-samples are conducted at the fixed gate voltages V_g corresponding to the first dip position on the hole-side of the $R_{xx}(V_g)$ curves. Here, the two different slopes of R_{xy} in the low B -field regime ($B < 4 \text{ T}$) represent different carrier densities. According to the inset showing the zoomed-region, we find that R_{xy} in our patched graphene starts saturating to quantum Hall plateau from $B \approx 11 \text{ T}$, while non-patched graphene converges to it from $B \approx 10 \text{ T}$. The variation of plateau values between the two cases is much likely due to different contact resistances in each measurement. Indeed, the part of the current that branches off into the shunt resistors depends on the contact resistances rather than the quality of graphene.

It is interesting that QHE is developed even in such low mobility CVD-graphene where highly defective multilayer graphene patches are dispersed. Although there are reports on QHE in CVD-graphene grown on Ni⁷ and Cu,¹² the graphene mobility is usually larger than $3000 \text{ cm}^2\text{V}^{-1}\text{s}^{-1}$ associated with less defects (also witnessed by a small Raman D-band). According to the Raman spectra in Fig. 1(d), the mobility of graphene in the single layer region can be estimated to be $\sim 3000 \text{ cm}^2\text{V}^{-1}\text{s}^{-1}$.²⁶ In principle, the mobility is high enough to validate the QHE so that our observation of QHE in the (on average) low-mobility sample can be ascribed to the locally high mobility graphene. This is in agreement with in general higher quality of CVD-graphene grown on Pt.

Indeed, recent study shows that graphene grown on Pt can have millimetre-sized hexagonal single-crystal grains with mobility greater than $7100 \text{ cm}^2\text{V}^{-1}\text{s}^{-1}$,¹⁴ which implies superior graphene quality compared to previously reported CVD-graphene using other metal catalysts. Additionally, we use the bubbling transfer technique^{14,18} instead of wet etching. This technique allows avoiding etchant residues and getting cleaner graphene surface. Therefore, Pt catalyst combined with bubbling transfer can be favourable for QHE behaviour.

Based on the measurements of R_{xx} and R_{xy} in Figs. 2(a) and 2(b), we show the longitudinal (σ_{xx})- and Hall (σ_{xy}) conductivities in Fig. 3 as functions of the carrier density n ($= \beta(V_g - V_{DP})$, where $\beta \approx 6.7 \times 10^{10} \text{ cm}^{-2} \text{ V}^{-1}$), obtained

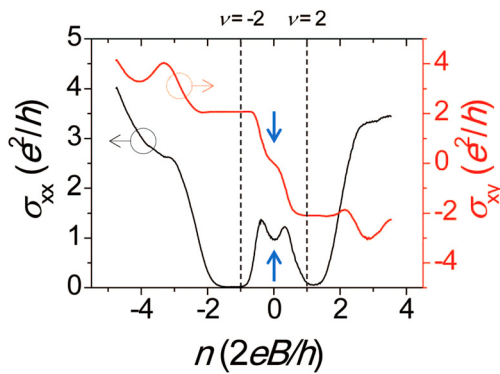


FIG. 3. The longitudinal conductivity σ_{xx} (black lines) and Hall conductivity σ_{xy} (red lines) versus the carrier density n . They are calculated using R_{xx} and R_{xy} in Figs. 2(a) and 2(b). The n corresponding to filling factor $\nu = \pm 2$ are denoted as vertical dashed lines. Two vertical blue arrows indicate unusual dip (in σ_{xx}) and plateau (in σ_{xy}) at $n = 0$.

from Hall measurement) measured in units of $2eB/h$ which correspond to the half of filling factor $\nu/2$ ($=hn/2eB$). Here, h and e are the Plank's constant and electron charge, respectively. Apart from the expected quantum Hall conductivity plateaus at $\pm 2e^2/h$, we see other features. First, at the Dirac point ($n = 0$), σ_{xx} shows an unexpected dip while σ_{xy} has an unusual Hall plateau as indicated by the two vertical blue arrows in Fig. 3. This can be attributed to a band gap formation at the Dirac point resulting in a slight splitting of the central LL at $n = 0$ into two levels. Until now, the $\nu = 0$ quantum Hall state has been experimentally observed only for high quality graphene made by mechanical exfoliation.^{4,5,27–29} This state is normally explained by the spin-valley symmetry breaking which lifts the degeneracy of LL,^{4,29} counter-propagating edge states,²⁷ and gap opening in the magnetic field.^{5,28} We believe that in our case it is rather due to the disorder induced gap opening³⁰ resulting from the defective multilayer graphene patches. In fact, we also observed the same behaviour of the QHE in wrinkled CVD-graphene grown on Cu (not shown here).

Moreover, the centre of the dip (in σ_{xx}) and plateau (in σ_{xy}) is somewhat shifted from the anticipated positions $\nu = \pm 2$ denoted by the vertical dashed lines. This can be attributed to a pool of localized states which do not contribute to the degeneracy of LL.³¹ The localized states are situated between LLs and result in a “delay” when filling LLs by increasing carrier density. Here, the spatially distributed graphene patches probably act as origin of the localized states.

We have observed the QHE in CVD-graphene grown on platinum. The QHE is even seen in samples which are irregularly decorated with disordered multilayer graphene patches and have very low mobility ($< 500 \text{ cm}^2\text{V}^{-1}\text{s}^{-1}$). The effect does not seem to depend on electronic mobility and uniformity of the resulting material, which indicates the robustness of QHE in graphene.

Financial support from the Swedish Research Council, the Swedish Foundation for Strategic Research (Sweden), and the Leading Foreign Research Institute Recruitment Program (No. 0409-20100156) of National Research Foundation and the FPRD of BK21 through the Ministry of Education, Science and Technology, Korea is greatly appreciated.

Clean-room processing has been achieved using equipment sponsored by the Knut and Alice Wallenberg Foundation.

- ¹K. v. Klitzing, G. Dorda, and M. Pepper, *Phys. Rev. Lett.* **45**(6), 494 (1980); T. Ando, A. B. Fowler, and F. Stern, *Rev. Mod. Phys.* **54**(2), 437 (1982).
- ²K. S. Novoselov, A. K. Geim, S. V. Morozov, D. Jiang, Y. Zhang, S. V. Dubonos, I. V. Grigorieva, and A. A. Firsov, *Science* **306**(5696), 666 (2004).
- ³K. S. Novoselov, A. K. Geim, S. V. Morozov, D. Jiang, M. I. Katsnelson, I. V. Grigorieva, S. V. Dubonos, and A. A. Firsov, *Nature* **438**(7065), 197 (2005); Y. Zhang, Y.-W. Tan, H. L. Stormer, and P. Kim, *ibid.* **438**(7065), 201 (2005).
- ⁴Y. Zhang, Z. Jiang, J. P. Small, M. S. Purewal, Y. W. Tan, M. Fazlollahi, J. D. Chudow, J. A. Jaszczak, H. L. Stormer, and P. Kim, *Phys. Rev. Lett.* **96**(13), 136806 (2006).
- ⁵J. G. Checkelsky, L. Li, and N. P. Ong, *Phys. Rev. Lett.* **100**(20), 206801 (2008).
- ⁶X. Du, I. Skachko, F. Duerr, A. Luican, and E. Y. Andrei, *Nature* **462**(7270), 192 (2009); C. R. Dean, A. F. Young, P. Cadden-Zimansky, L. Wang, H. Ren, K. Watanabe, T. Taniguchi, P. Kim, J. Hone, and K. L. Shepard, *Nat. Phys.* **7**(9), 693 (2011).
- ⁷K. I. Bolotin, F. Ghahari, M. D. Shulman, H. L. Stormer, and P. Kim, *Nature* **462**(7270), 196 (2009).
- ⁸K. S. Novoselov, Z. Jiang, Y. Zhang, S. V. Morozov, H. L. Stormer, U. Zeitler, J. C. Maan, G. S. Boebinger, P. Kim, and A. K. Geim, *Science* **315**(5817), 1379 (2007).
- ⁹Y. G. Arapov, G. I. Harus, I. V. Karskanov, V. N. Neverov, N. G. Shelushinina, M. V. Yakunin, O. A. Kuznetsov, L. Ponomarenko, and A. de Visser, *Low Temp. Phys.* **33**(2), 147 (2007); C.-T. Liang, L.-H. Lin, C. K. Yoa, S.-T. Lo, Y.-T. Wang, D.-S. Lou, G.-H. Kim, C. Yuan-Huei, Y. Ochiai, N. Aoki, J.-C. Chen, Y. Lin, H. Chun-Feng, S.-D. Lin, and D. Ritchie, *Nanoscale Res. Lett.* **6**(1), 131 (2011).
- ¹⁰E. Pallecchi, M. Ridene, D. Kazazis, F. Lafont, F. Schopfer, W. Poirier, M. O. Goerbig, D. Maily, and A. Ouerghi, *Sci. Rep.* **3**, 1791 (2013).
- ¹¹K. S. Kim, Y. Zhao, H. Jang, S. Y. Lee, J. M. Kim, K. S. Kim, J.-H. Ahn, P. Kim, J.-Y. Choi, and B. H. Hong, *Nature* **457**(7230), 706 (2009).
- ¹²S. Bae, H. Kim, Y. Lee, X. Xu, J.-S. Park, Y. Zheng, J. Balakrishnan, T. Lei, H. R. Kim, Y. I. Song, Y.-J. Kim, K. S. Kim, B. Ozyilmaz, J.-H. Ahn, B. H. Hong, and S. Iijima, *Nat. Nanotechnol.* **5**(8), 574 (2010); H. Cao, Q. Yu, L. A. Jauregui, J. Tian, W. Wu, Z. Liu, R. Jalilian, D. K. Benjamin, Z. Jiang, J. Bao, S. S. Pei, and Yong P. Chen, *Appl. Phys. Lett.* **96**(12), 122106 (2010); T. Shen, W. Wu, Q. Yu, C. A. Richter, R. Elmquist, D. Newell, and Y. P. Chen, *ibid.* **99**(23), 232110 (2011).
- ¹³P. Sutter, J. T. Sadowski, and E. Sutter, *Phys. Rev. B* **80**(24), 245411 (2009); J. Ping and M. S. Fuhrer, e-print [arXiv:1304.5123](https://arxiv.org/abs/1304.5123).
- ¹⁴L. Gao, W. Ren, H. Xu, L. Jin, Z. Wang, T. Ma, L.-P. Ma, Z. Zhang, Q. Fu, L.-M. Peng, X. Bao, and H.-M. Cheng, *Nat. Commun.* **3**, 699 (2012).
- ¹⁵H. Xu, Z. Zhang, R. Shi, H. Liu, Z. Wang, S. Wang, and L.-M. Peng, *Sci. Rep.* **3**, 1207 (2013); R. Shi, H. Xu, B. Chen, Z. Zhang, and L.-M. Peng, *Appl. Phys. Lett.* **102**(11), 113102 (2013).
- ¹⁶S. Jie, N. Lindvall, M. T. Cole, K. T. T. Angel, W. Teng, K. B. K. Teo, D. H. C. Chua, L. Johan, and A. Yurgens, *IEEE Trans. Nanotechnol.* **11**(2), 255 (2012).
- ¹⁷For instance, the nominal value corresponding to Cu melting point is about 850°C . Therefore, we believe actual temperature in the case of Pt catalyst is also somewhat higher than 1000°C .
- ¹⁸C. J. L. de la Rosa, J. Sun, N. Lindvall, M. T. Cole, Y. Nam, M. Loffler, E. Olsson, K. B. K. Teo, and A. Yurgens, *Appl. Phys. Lett.* **102**(2), 022101 (2013).
- ¹⁹D. C. Elias, R. R. Nair, T. M. G. Mohiuddin, S. V. Morozov, P. Blake, M. P. Halsall, A. C. Ferrari, D. W. Boukhvalov, M. I. Katsnelson, A. K. Geim, and K. S. Novoselov, *Science* **323**(5914), 610 (2009).
- ²⁰J.-H. Chen, W. G. Cullen, C. Jang, M. S. Fuhrer, and E. D. Williams, *Phys. Rev. Lett.* **102**(23), 236805 (2009).
- ²¹A. B. Kaiser, C. Gómez-Navarro, R. S. Sundaram, M. Burghard, and K. Kern, *Nano Lett.* **9**(5), 1787 (2009).
- ²²W. Zhu, V. Perebeinos, M. Freitag, and P. Avouris, *Phys. Rev. B* **80**(23), 235402 (2009).
- ²³J. Hong, M. K. Park, E. J. Lee, D. Lee, D. S. Hwang, and S. Ryu, *Sci. Rep.* **3**, 2700 (2013).
- ²⁴E. H. M. Ferreira, M. V. O. Moutinho, F. Stavale, M. M. Lucchese, R. B. Capaz, C. A. Achete, and A. Jorio, *Phys. Rev. B* **82**(12), 125429 (2010).

- ²⁵T. Löfwander, P. San-Jose, and E. Prada, *Phys. Rev. B* **87**(20), 205429 (2013).
- ²⁶Z. H. Ni, L. A. Ponomarenko, R. R. Nair, R. Yang, S. Anissimova, I. V. Grigorieva, F. Schedin, P. Blake, Z. X. Shen, E. H. Hill, K. S. Novoselov, and A. K. Geim, *Nano Lett.* **10**(10), 3868 (2010).
- ²⁷D. A. Abanin, K. S. Novoselov, U. Zeitler, P. A. Lee, A. K. Geim, and L. S. Levitov, *Phys. Rev. Lett.* **98**(19), 196806 (2007).
- ²⁸L. Zhang, Y. Zhang, M. Khodas, T. Valla, and I. A. Zaliznyak, *Phys. Rev. Lett.* **105**(4), 046804 (2010).
- ²⁹Y. Zhao, P. Cadden-Zimansky, F. Ghahari, and P. Kim, *Phys. Rev. Lett.* **108**(10), 106804 (2012).
- ³⁰C.-K. Yang, *Carbon* **48**(13), 3901 (2010); B. S. Pujari and D. G. Kanhere, *J. Phys. Chem. C* **113**(50), 21063 (2009); N. Amirhasan, C. Mirco, V. Tom, P. Geoffrey, C. Francesca, H. van der Veen Marleen, H. Johan, M. H. Marc, G. Stefan De, and F. S. Bert, *Nanotechnology* **21**(43), 435203 (2010).
- ³¹D. S. Lee, C. Riedl, T. Beringer, A. H. C. Neto, K. von Klitzing, U. Starke, and J. H. Smet, *Phys. Rev. Lett.* **107**(21), 216602 (2011).